SCIENCE CHINA
Earth Sciences

• RESEARCH PAPER •

May 2016 Vol.59 No.5: 989–996
doi: 10.1007/s11430-016-5269-9

Compressional behavior of $MgCr_2O_4$ spinel from first-principles simulation

ZHANG YanYao[1,2], LIU Xi[1,2*], XIONG ZhiHua[1,2] & ZHANG ZhiGang[3]

[1] *Key Laboratory of Orogenic Belts and Crustal Evolution, Ministry of Education of China, Beijing 100871, China;*
[2] *School of Earth and Space Sciences, Peking University, Beijing 100871, China;*
[3] *Key Laboratory of Earth and Planetary Physics, Institute of Geology and Geophysics, Chinese Academy of Sciences, Beijing 100029, China*

Received September 22, 2015; accepted December 28, 2015; published online March 4, 2016

Abstract The compressional behavior of the $MgCr_2O_4$ spinel has been investigated with the CASTEP code using density functional theory and planewave pseudopotential technique. We treated the exchange-correlation interaction by both the local density approximation (LDA) and generalized gradient approximation (GGA) with the Perdew-Burker-Ernzerhof functional. Our simulation was conducted for the pressure range of 0–19 GPa. We obtained the isothermal bulk modulus (K_T) of the $MgCr_2O_4$ spinel as 181.46(48) GPa (GGA; low boundary) or 216.1(11) GPa (LDA; high boundary), with its first derivative (K_T') as 4.41(6) or 4.5(1), respectively. The oxygen parameter u is not constant but negatively correlated with P, and decreases by about 0.5–0.6% for the investigated P range. The component polyhedra have different compressibilities, increasing in the order of $(O_4)_1$<CrO_6<$(O_4)_2$<O_6<MgO_4. The Mg-O bond in the MgO_4 tetrahedron is much more compressible than the Cr-O bond in the CrO_6 octahedron.

Keywords $MgCr_2O_4$ spinel, Compressional behavior, GGA, LDA, Polyhedral compressibility

Citation: Zhang Y Y, Liu X, Xiong Z H, Zhang Z G. 2016. Compressional behavior of $MgCr_2O_4$ spinel from first-principles simulation. Science China Earth Sciences, 59: 989−996, doi: 10.1007/s11430-016-5269-9

1. Introduction

Chromium spinels are commonly found in the Earth's crust and upper mantle (Cookenboo et al., 1997; Barnes and Roeder, 2001; Yang et al., 2007). They present as accessory phases, but are widely considered to be significant petrogenetic indicators to geological processes such as the crystallizing process of mantle-derived magma (Barnes and Roeder, 2001), the partial melting activity of the upper mantle (Dick and Bullen, 1984; Liu and O'Neill, 2004), and the metamorphic evolution of some ore deposits (Graham, 1978; Paraskevopoulos and Economou, 1981). They have great potentials to be used as geothermometer (Fabries, 1979; Ballhaus et al., 1990), geobarometer (O'Neill, 1981; O'Neill and Wall, 1987) and oxygen barometer (Ballhaus et al., 1991) in rocks. Among the chromium spinels, magnesiochromite ($MgCr_2O_4$) is the only ore mineral of chromium (Duke, 1983), and is an important mineral inclusion in cratonic diamonds (Stachel and Harris, 2008). In addition, it is a commercially important refractory material for some technological applications (Karklit et al., 1970). Therefore, its physical and chemical properties have attracted considerable attention and been investigated in many studies (O'Neill and Navrotsky, 1983; O'Neill and Dollase, 1994; Klemme and O'Neill, 1997; Catti et al., 1999; Wang et al., 2002; Ottonello et al., 2007; Yong et al., 2012; Wang et al., 2012; Nestola et al., 2014).

Magnesiochromite is cubic and has the space group $Fd\bar{3}m$ (No. 227; Z=8). Its Mg^{2+} and Cr^{3+} cations occupy

*Corresponding author (email: xi.liu@pku.edu.cn)

one eighth of the tetrahedral (8*a*) sites and half of the octahedral (16*d*) sites, respectively. Its oxygens form a quasi-ideal close-packed *fcc* structure (equipoint 32*e*), and their full description requires an additional parameter, the oxygen parameter (or internal parameter) *u*. For an ideal cubic close-packing of oxygens in the spinels, *u* is 0.25. The *u* parameter of the $MgCr_2O_4$ spinel is around 0.2604–0.2620 (Hill et al., 1979; O'Neill and Navrotsky, 1983; O'Neill and Dollase, 1994; Lenaz et al., 2004).

The isothermal bulk modulus (K_T) of the $MgCr_2O_4$ spinel was experimentally investigated by Yong et al. (2012) and Nestola et al. (2014), and theoretically investigated by Catti et al. (1999) and Ottonello et al. (2007). Nestola et al. (2014) gave out a smaller K_T value (189.6(7) GPa, with the first derivative of the K_T, K_T', fixed as 4) than Yong et al. (2012) (206.9(19) GPa, with K_T' fixed as 4). In contrast, the two theoretical studies using similar functionals of exchange-correlation energy obtained similar results (197.3 and 192.56 GPa). On the other hand, the compression behavior of the component polyhedra and cation-oxygen bonds under hydrostatic pressure has not been studied.

In order to constrain the K_T value of the $MgCr_2O_4$ spinel, we have performed new first-principles simulation with different functionals of exchange-correlation energy. On the basis of our first-principles simulation, we have further decomposed the bulk compressibility into polyhedral terms, and systematically explored the contributions of the polyhedra to the compressibility of the $MgCr_2O_4$ spinel. Finally, we have compared the compressibilities of the Mg-O bond and Cr-O bond in the MgO_4 tetrahedron and CrO_6 octahedron, respectively.

2. Simulating methods

Our investigations on the bulk modulus of the magnesiochromite were based on the application of the Density Functional Theory (DFT) (Hohenberg and Kohn, 1964; Kohn and Sham, 1965) and planewave pseudopotential technique (Payne et al., 1992) implemented in the CASTEP code. We treated the exchange-correlation interaction by both the local density approximation (LDA) (Ceperley and Alder, 1980; Perdew and Zunger, 1981) and generalized gradient approximation (GGA) with the Perdew-Burker-Ernzerhof functional (Perdew et al., 1996), and used a convergence criterion of 10^{-6} eV/atom on the total energy in the self-consistent field calculations. We employed a planewave basis set with a cutoff of 1000 eV to expand the electronic wave functions, and a norm-conserving pseudopotential to model the ion-electron interaction (Lin et al., 1993; Lee, 1995). We sampled the irreducible Brillouin zone with a 2×2×2 Monkhorst-Pack grid (Monkhorst and Pack, 1976). The effects of using larger cutoff and k point mesh on the calculated properties were found to be insignificant.

The initial structure model used in our simulation was from O'Neill and Dollase (1994). The computation cell contained eight $MgCr_2O_4$ molecules, that is, in total 56 atoms. The equilibrium lattice parameters and internal coordinates at different pressures were optimized by minimizing the Hellmann-Feynman force on the atoms and simultaneously matching the stress on the unit-cell to the target stress. After the final self-consistency cycle, the remaining Hellmann-Feynman forces on the atoms were typically <0.03 eV/Å and the remaining stress was <0.05 GPa. The geometry optimizing was conducted from 0 to 19 GPa at 0 K. In this range of pressure, any decomposition or phase transition of the magnesiochromite should not occur according to previous theoretical and experimental studies (Catti et al., 1999; Yong et al., 2012).

3. Result and discussion

Comparison of the theoretically-calculated geometry parameters (a_0, V_0, and u_0) at zero pressure with the experimentally-determined unit-cell parameters at ambient condition by O'Neill and Dollase (1994) is shown in Table 1. Our data present slight overestimation of a_0 and V_0 (0.60% and 1.83%, respectively) with the GGA method, but slight underestimation of a_0 and V_0 (–1.38% and –4.07%, respectively) with the LDA method. These phenomena are typical for the GGA and LDA method (Chang et al., 2013; Rodríguez-Hernández and Muñoz, 2014). Additionally, the calculated oxygen parameter *u* is smaller by –0.56% or –0.99% using the GGA or LDA method, respectively. Summarily, both methods reproduce well the geometry parameters of the $MgCr_2O_4$ spinel.

The calculated cell parameters at each pressure are reported in Table 2. As *P* increases from 0 to 19 GPa, the unit-cell lattice parameter *a* decreases from 8.3845

Table 1 Comparison between experimental and energy-optimized crystallographic data of the $MgCr_2O_4$ spinel [a)]

Parameters	Experimental	Calculated by first-principles simulation			
		GGA	R.D. (%)	LDA	R.D. (%)
a_0 (Å)	8.3341	8.3845	0.60	8.2195	–1.38
V_0 (Å^3)	578.863	589.438	1.83	555.314	–4.07
u_0	0.26070	0.25924	–0.56	0.25812	–0.99

a) Experimental refer to O'Neill and Dollase (1994); R.D., relative difference.

Table 2 Calculated unit-cell parameters at different pressures

P (GPa)	GGA				LDA			
	a (Å)	*V* (Å^3)	*V*/*V*$_0$	*u*	*a* (Å)	*V* (Å^3)	*V*/*V*$_0$	*u*
0.0	8.3845	589.438	1.000	0.25924	8.2195	555.314	1.000	0.25812
1.0	8.3705	586.473	0.995	0.25917	8.2067	552.721	0.995	0.25804
3.0	8.3401	580.123	0.984	0.25897	8.1821	547.771	0.986	0.25788
5.0	8.3127	574.413	0.975	0.25882	8.1591	543.154	0.978	0.25773
7.0	8.2857	568.840	0.965	0.25862	8.1366	538.685	0.970	0.25758
9.0	8.2597	563.492	0.956	0.25848	8.1152	534.444	0.962	0.25744
11.0	8.2350	558.468	0.947	0.25833	8.0944	530.335	0.955	0.25731
13.0	8.2124	553.877	0.940	0.25818	8.0748	526.489	0.948	0.25719
15.0	8.1897	549.295	0.932	0.25805	8.0548	522.590	0.941	0.25703
17.0	8.1673	544.789	0.924	0.25791	8.0358	518.896	0.934	0.25692
19.0	8.1465	540.639	0.917	0.25779	8.0177	515.398	0.928	0.25680

to 8.1465 Å (by 2.84%; GGA) or 8.2195 to 8.0177 Å (by 2.46%; LDA), the volume decreases from 589.438 to 540.639 Å^3 (by 8.28%; GGA) or 555.314 to 515.398 Å^3 (by 7.19%; LDA), and the oxygen parameter *u* decreases from 0.25924 to 0.25779 (by 0.56%; GGA) or 0.25812 to 0.25680 (by 0.51%; LDA).

The calculated *P*-*V* data have been fitted to the third-order Birch-Murnaghan equation of state (BM-EoS; Birch, 1947) by a least-squares method to determine the isothermal bulk modulus:

$$P=\frac{3K_T}{2}\left[\left(\frac{V_0}{V}\right)^{7/3}-\left(\frac{V_0}{V}\right)^{5/3}\right]\times\left\{1+\frac{3(K_T'-4)}{4}\left[\left(\frac{V_0}{V}\right)^{2/3}-1\right]\right\}, \quad (1)$$

where *P* and *V* are the calculated pressure and unit-cell volume, respectively. K_T, K_T', and V_0 are the bulk modulus, its pressure derivative, and the unit-cell volume at zero pressure, respectively. Using the *P*-*V* data from the GGA method, we have obtained the following BM-EoS parameters for the $MgCr_2O_4$ spinel: K_T=181.46(48) GPa, K_T'=4.41(6), V_0=589.48(3) Å^3; using the *P*-*V* data from the LDA method, we have obtained the following BM-EoS parameters: K_T=216.1(11) GPa, K_T'=4.5(1), V_0=555.22(4) Å^3. The K'_T value of the $MgCr_2O_4$ spinel was suggested as ~4 in Catti et al. (1999) and Ottonello et al. (2007). With the assumption of K_T'=4, we obtain the following results: K_T=184.93(37) GPa and V_0=589.34(6) Å^3 (GGA), and K_T=220.50(52) GPa and V_0=555.10(6) Å^3 (LDA).

The normalized volumes of the $MgCr_2O_4$ spinel at different pressures predicted by our first-principles simulation are shown along with the experimentally-obtained data in Figure 1. Compared to the experimentally-determined curves, the curve obtained with the GGA method has a slightly steeper slope whereas that obtained with the LDA method has a more gradual slope. In general, the GGA method

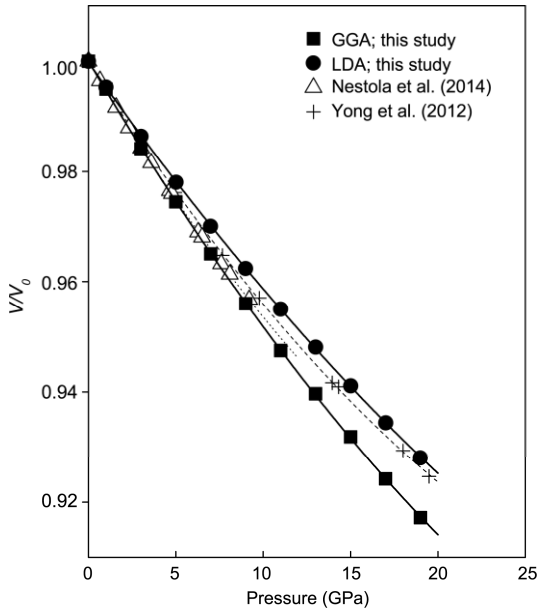

Figure 1 Normalized bulk volume (*V*/*V*$_0$) versus pressure (*P*).

should yield a lower K_T and the LDA method should yield a higher K_T, with the experimentally-constrained K_T falling in between (Deng et al., 2011). The *V*/*V*$_0$-*P* trend from Nestola et al. (2014) is much closer to our GGA result, while the *V*/*V*$_0$-*P* trend from Yong et al. (2012) is much closer to our LDA result. Consequently, the K_T value of the $MgCr_2O_4$ spinel suggested by Nestola et al. (2014) is close to our GGA result while that by Yong et al. (2012) is close to our LDA result (Table 3).

Catti et al. (1999) and Ottonello et al. (2007) theoretically obtained the K_T values of the $MgCr_2O_4$ spinel as 197.3 and 192.56 GPa, respectively. They used either the HF functional or the hybrid B3LYP functional to approximate the correlation energy (Becke, 1993; Stephens et al., 1994), so that their results are different to our results but fall between

Table 3 Equation of state of the $MgCr_2O_4$ spinel[a)]

K_T (GPa)	K'_T	V_0 (Å^3)	Method	Data source
181.46(48)	4.41(6)	589.48(3)	The/DFT/GGA/1000	This study
184.93(37)	4[b)]	589.34(6)	The/DFT/GGA/1000	This study
216.1(11)	4.5(1)	555.22(4)	The/DFT/LDA/1000	This study
220.50(52)	4[b)]	555.10(6)	The/DFT/LDA/1000	This study
182.5(14)	5.8(4)	579.30(4)	Exp/CX/SC/EM/Quartz	Nestola et al. (2014)
189.6(7)	4[b)]	579.16(5)	Exp/CX/SC/EM/Quartz	Nestola et al. (2014)
189(2)	7.2(3)	578.68(4)	Exp/SX/Powder/Ar/Gold	Yong et al. (2012)
206.9(19)	4[b)]	578.66(8)	Exp/SX/Powder/Ar/Gold	Yong et al. (2012)
192.56	4.066	–	The/DFT/B3LYP	Ottonello et al. (2007)
197.3	3.94	–	The/DFT/HF	Catti et al. (1999)

a) Some details of the simulating methods and experimental techniques. The, theoretical; DFT, density functional theory; GGA, generalized gradient approximation; LDA, local density approximation; B3LYP, hybrid B3LYP functional; HF, hartree-fock functional; 1000, cutoff energy of 1000 eV; Exp, experimental; CX, conventional X-ray; SX, synchrotron X-ray; SC, single crystal; Powder, powder sample; EM, pressure medium of an 1:4 ethanol-methanol mixture; Ar, pressure medium of Argon; Quartz, pressure scale of Quartz (Angel et al., 1997); Gold, pressure scale of Gold (Fei et al., 2007). b) Fixed as 4.

the results from the GGA and LDA method (Table 3).

By fixing the K'_T to different values and calculating the K_T, a correlation analysis of the K_T and K'_T has been carried out, and the result is shown in Figure 2. The K_T value decreases from 203(2) to 142(4) GPa (GGA) or from 239(2) to 176(4) GPa (LDA) as the K'_T value increases from 2 to 10, with the previous experimentally and theoretically obtained K_T values generally falling in between.

The relationship between the parameter u and the $d_{M\text{-}O}/d_{T\text{-}O}$ ratio (R; $d_{M\text{-}O}$ and $d_{T\text{-}O}$ representing the averaged bond length of the octahedron and tetrahedron, respectively) can be described by the following equation (Hill et al., 1979):

$$u = \frac{R^2/4 - 2/3 + \left(11R^2/48 - 1/18\right)^{1/2}}{2R^2 - 2}. \quad (2)$$

A constant u value at different pressures means equal compressibility of the octahedra and tetrahedra, whereas a negative correlation between the parameter u and P corresponds to a greater compressibility of the tetrahedra and *vice verse*. In the case of the $MgCr_2O_4$ spinel, the oxygen parameter u decreases as P increases from zero pressure to 19 GPa (Table 2). Regression of these data gives u=0.259–9.307×10^{-5} P+8.525×10^{-7} P^2 (GPa) for the GGA method or u=0.258–7.961×10^{-5} P+5.432×10^{-7} P^2 (GPa) for the LDA method (Figure 3). It follows that as P increases, the MgO_4 tetrahedra in the $MgCr_2O_4$ spinel are more compressible than the CrO_6 octahedra, so that the oxygens move closer to the nearest tetrahedral Mg^{2+} along the [111] direction and form a less distorted close-packing arrangement, and the CrO_6 octahedra become less distorted (Hill et al., 1979; Recio et al., 2001; Gracia et al., 2002; Bouhemadou et al., 2007; Rodríguez-Hernández and Muñoz, 2014).

The reaction of the $MgCr_2O_4$ spinel under pressure depends

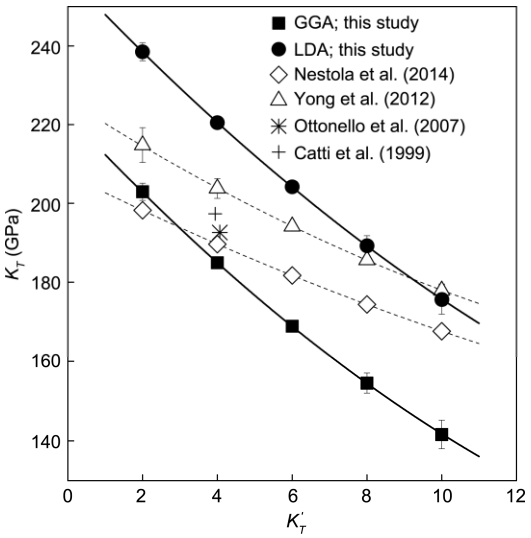

Figure 2 Isothermal bulk modulus (K_T) versus its pressure derivative (K'_T).

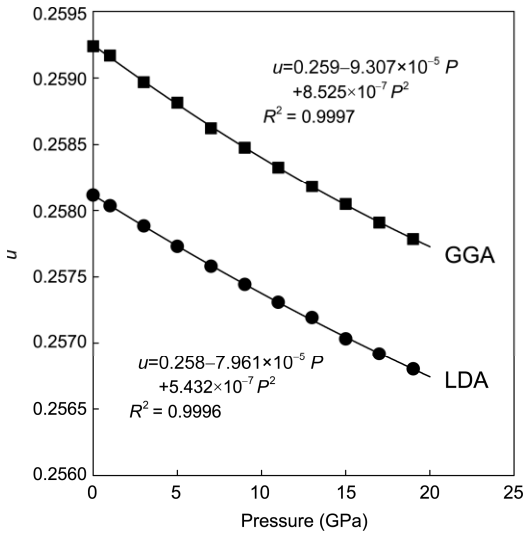

Figure 3 Oxygen parameter (u) versus pressure (P).

on the different pressure response of the component polyhedra and the manner in which these polyhedra are linked (Hazen and Finger, 1979). According to Gracia et al. (2002), the unit cell of the spinel structure can be completely divided into five types of polyhedra without any overlapping: CrO_6, MgO_4, O_6, $(O_4)_1$, and $(O_4)_2$, with multiplicities n_P=16, 8, 16, 8, and 48, respectively (Figure 4). These polyhedra are linked via extensive edge sharing in three dimensions (Hazen and Finger, 1979). The volumes of these component polyhedra (V_P) can be expressed as simple algebraic functions of the unit-cell volume (V) and the oxygen parameter (u; Yamanaka and Takéuchi, 1983):

$$\begin{aligned} V_{\mathrm{CrO_6}} &= 128V\cdot u\cdot u_{38}^2/3,\\ V_{\mathrm{MgO_4}} &= 64V\cdot |u_{18}|^3/3,\\ V_{\mathrm{O_6}} &= 128V\cdot u_{18}^2\cdot |u_{12}|/3,\\ V_{(\mathrm{O_4})_1} &= 64V\cdot |u_{38}|^3/3,\\ V_{(\mathrm{O_4})_2} &= 8V\cdot |u_{18}|\cdot |u_{38}|/3, \end{aligned} \tag{3}$$

where $u_{ij}=u-i/j$. The isothermal polyhedral compressibilities (κ_P) are the inverse of the polyhedral bulk moduli (K_P),

$$\kappa_P=\frac{1}{K_P}=-\frac{1}{V_P}\left(\frac{\partial V_P}{\partial P}\right), \tag{4}$$

and they can be written in the general form as follows:

$$\kappa_P=\kappa-g_P\left(\frac{\partial u}{\partial P}\right). \tag{5}$$

The g_P term in eq. (5) is the structural coefficient of the polyhedral-bulk compressibility relation (Hazen and Finger, 1979),

$$\begin{aligned} g_{\mathrm{CrO_6}} &= 1/u+2/u_{38},\\ g_{\mathrm{MgO_4}} &= 3/u_{18},\\ g_{\mathrm{O_6}} &= 2/u_{18}+1/u_{12},\\ g_{(\mathrm{O_4})_1} &= 3/u_{38},\\ g_{(\mathrm{O_4})_2} &= 1/u_{18}+1/u_{38}. \end{aligned} \tag{6}$$

The bulk compressibility (κ) then is a weighted sum of the polyhedral contributions:

$$\kappa=\sum_p f_P\kappa_P, \tag{7}$$

where f_P represents the volumetric fraction of the component polyhedra in the unit cell:

$$f_P=\frac{n_P V_P}{V}. \tag{8}$$

The zero-pressure response of the $MgCr_2O_4$ spinel to pressure, in terms of the component polyhedra, is presented in Table 4. All component polyhedra show different pressure responses, with their compressibilities in the order of $(O_4)_1$< CrO_6 <$(O_4)_2$<O_6<MgO_4 (Figure 5). According to eq. (5), if u remains constant with pressure, the *fcc* arrangement of the oxygens should not change, and the polyhedral and bulk compressibilities should be the same. Our calculated value for $(\partial u/\partial P)$ is -9.307×10^{-5} GPa^{-1} (GGA) or -7.961×10^{-5} GPa^{-1} (LDA). This number and the calculated zero-pressure g_p functions (Table 4) lead to the polyhedral bulk moduli K_P in the range from 132 to 323 GPa (GGA) or from 156 to 387 GPa (LDA). The polyhedra (CrO_6, $(O_4)_1$ and $(O_4)_2$) with volumes smaller than their corresponding volumes in an ideal *fcc* oxygen arrangement (u=0.25) have larger polyhedral bulk moduli than the bulk modulus of the $MgCr_2O_4$ spinel, and *vice verse* (MgO_4 and O_6; Table 4).

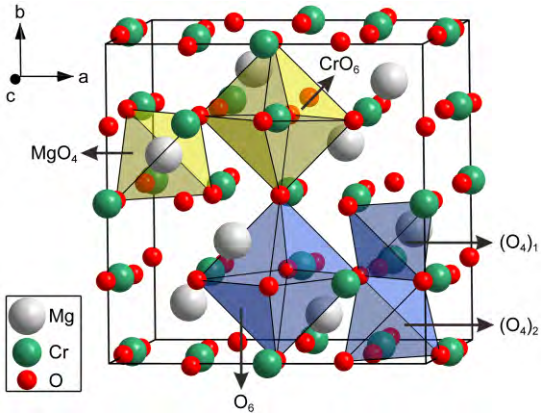

Figure 4 Polyhedra in the $MgCr_2O_4$ spinel structure (19 GPa; GGA method; see Table 2 for the details).

Polyhedral compressibilities are in general determined by bond-length compressibilities (D'Arco et al., 1991; Catti et al., 1999; Recio et al., 2001; Rodríguez-Hernández and Muñoz, 2014). According to Recio et al. (2001), the cation-anion bond lengths at the tetrahedral ($d_{\mathrm{Mg\text{-}O}}$) and octahedral ($d_{\mathrm{Cr\text{-}O}}$) sites can be obtained, respectively, by:

$$d_{\mathrm{Mg\text{-}O}}=\sqrt{3}a\left(u-\frac{1}{8}\right),\quad d_{\mathrm{Cr\text{-}O}}=a\sqrt{\left(u-\frac{1}{2}\right)^2+2\left(u-\frac{1}{4}\right)^2}, \tag{9}$$

where a stands for the unit-cell parameter and u for the oxygen parameter. Figure 6 depicts the variation of the normalized cation-oxygen bond lengths (d/d_0) under pressure, with the Mg-O bond decreasing by about 3.4–3.9% and the Cr-O bond by about 2.0–2.3% for the investigated P range. The Mg-O bond is therefore more compressible than the Cr-O bond, in good agreement with the relative compressibilities of the MgO_4 and CrO_6 polyhedron (Figure 5).

The magnesiochromite has been discovered as inclusion in diamonds originating from peridotitic mantle source (Stachel and Harris, 2008; Lenaz et al., 2009), which provides a means to explore the *P-T* conditions of the diamond formation (or the *P-T* condition for trapping the magnesio-

Table 4 Decomposition of the bulk compressibility into the component polyhedral contributions according to the first-principles simulation using the GGA and LDA method

	V_P (Å^3) GGA/LDA	n_P	f_P^{ideal}	f_P GGA/LDA	$\kappa_P\times10^{-3}$ (GPa^{-1}) GGA/LDA	g_P GGA/LDA	K_P (GPa) GGA/LDA
Unit cell	589.438/555.314		1	1/1	5.511/4.627		181.5/216.1
CrO_6	10.921/10.444	16	$\frac{1}{3}$	0.2964/0.3009	4.262/3.573	–13.420/–13.237	234.6/279.8
MgO_4	3.802/3.493	8	$\frac{1}{24}$	0.0516/0.0503	7.591/6.422	22.348/22.537	131.7/155.7
O_6	13.639/12.694	16	$\frac{1}{3}$	0.3702/0.3658	6.511/5.494	10.745/10.890	153.6/182.0
$(O_4)_1$	2.438/2.365	8	$\frac{1}{24}$	0.0331/0.0341	3.099/2.584	–25.915/–25.667	322.7/387.0
$(O_4)_2$	3.053/2.880	48	$\frac{1}{4}$	0.2486/0.2489	5.400/4.544	–1.189/–1.043	185.2/220.1

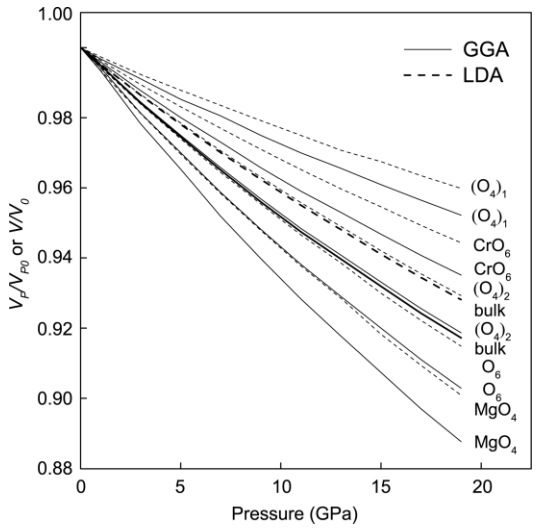

Figure 5 Relationship between the normalized polyhedral volume (V_P/V_{P0}) and pressure (P), compared to that between the normalized bulk volume (V/V_0) and pressure (P).

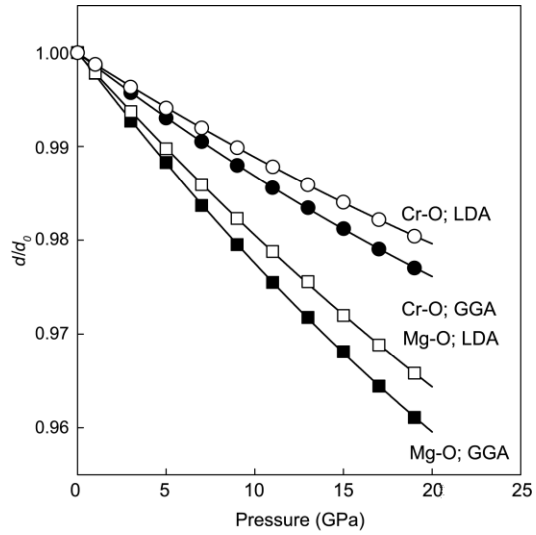

Figure 6 Normalized cation-oxygen bond lengths (d/d_0) versus pressure (P).

chromite). Based on the concept of the isovolume locus (Smith, 1953; Liu et al., 1990), Barron (2005) proposed an equation to estimate the *P*-*T* conditions as following

$$P_r=\{T(A_h-A_i)-P(B_h-B_i)\}/B_i, \quad (10)$$

where P_r, T, and P are residual pressure, temperature and pressure at the formation of the diamond, respectively; A_h, B_h, A_i, and B_i are thermal expansions and compressibilities of the host diamond and its inclusion, respectively. Using eq. (10), and with the thermal expansion and compressibility data for diamond used by Kagi et al. (2009; 7.08×10^{-7}°C^{-1} and 2.38×10^{-3} GPa^{-1}, respectively) and those for the magnesiochromite from Wang et al. (2012; 1.99×10^{-5}°C^{-1}) and this study, the *P*-*T* trajectory (*P*, GPa; *T*, K) for the diamonds to trap the magnesiochromite inclusions has been calculated as

$$P=0.0061T+1.76P_r, \quad (11a)$$

or

$$P=0.0085T+2.06P_r, \quad (11b)$$

where the compressibility of the magnesiochromite constrained by the GGA method (eq. (11a)) or LDA method (eq. (11b)) has been used in the calculation. The P_r can be obtained by using three different techniques: (1) microRaman spectroscopy (Nasdala et al., 2003); (2) strain birefringence analysis (Howell et al., 2010), and (3) single-crystal X-ray diffraction (Nestola et al., 2012). The formation *P* of the diamond host can then be determined, as long as its formation *T* independently estimated from some geothermometer or assumed from some typical geotherm (Barron, 2005; Xiong et al., 2016). Since the magnesiochromite inclusion in the diamonds usually coexists with chromite ($FeCr_2O_4$), hercynite ($FeAl_2O_4$), magnesioferrite ($MgFe_2O_4$) or magnetite (Fe_3O_4) (Lenaz et al., 2009), on the other hand, the formation *P* of the diamond can be actually constrained without any extra estimate of its formation *T* (Kagi et al., 2009).

4. Conclusions

With some first-principles simulations, we have obtained the following conclusions on the compressional behavior of the $MgCr_2O_4$ spinel.

(1) The K_T value of the $MgCr_2O_4$ spinel is 181.46(48) GPa (GGA; low boundary) or 216.1(11) GPa (LDA; high boundary), with its K'_T as 4.41(6) or 4.5(1), respectively.

(2) The oxygen parameter u is not constant but negatively correlated with P, $u=0.259-9.307\times10^{-5}P+8.525\times10^{-7}P^2$ (GPa; GGA) or $u=0.258-7.961\times10^{-5}P+5.432\times10^{-7}P^2$ (GPa; LDA).

(3) The component polyhedra have different compressibilities, with their volume reduction in the order of $(O_4)_1<CrO_6<(O_4)_2<O_6<MgO_4$. The Mg-O bond in the MgO_4 tetrahedron is much more compressible than the Cr-O bond in the CrO_6 octahedron.

Acknowledgements *We thank two anonymous scientists for providing very constructive comments. We thank editorial handling from Dr. Y. Zheng. This work was supported by the National Natural Science Foundation of China (Grant Nos. 41273072 and 41440015). The authors declare that they have no conflict of interest.*

References

Angel R J, Allan D R, Miletich R, Finger L W. 1997. The use of quartz as an internal pressure standard in high-pressure crystallography. J Appl Crystallogr, 30: 461–466

Ballhaus C, Berry R F, Green D H. 1990. Oxygen fugacity controls in the Earth's upper mantle. Nature, 349: 437–449

Ballhaus C, Berry R F, Green D H. 1991. High pressure experimental calibration of the olivine-orthopyroxene-spinel oxygen barometer: Implications for the oxidation state of the upper mantle. Contrib Mineral Petrol, 107: 27–40

Barnes S J, Roeder P L. 2001. The range of spinel compositions in terrestrial mafic and ultramafic rocks. J Petrol, 42: 2279–2302

Barron L M. 2005. A linear model and topography for the host-inclusion mineral system involving diamond. Can Mineral, 43: 203–224

Becke A D. 1993. Density-functional thermochemistry. III. The role of exact exchange. J Chem Phys, 98: 5648–5652

Birch F. 1947. Finite elastic strain of cubic crystals. Phys Rev, 71: 809–924

Bouhemadou A, Khenata R, Zerarga F. 2007. Ab initio study of the structural and elastic properties of spinels MgX_2O_4(X = Al, Ga, In) under pressure. Eur Phys J B, 56: 1–5

Catti M, Fava F F, Zicovich C, Dovesi R. 1999. High-pressure decomposition of MCr_2O_4 spinels (M = Mg, Mn, Zn) by ab initio methods. Phys Chem Miner, 26: 389–395

Ceperley D M, Alder B J. 1980. Ground state of the electron gas by a stochastic method. Phys Rev Lett, 45: 566–569

Chang L L, Liu X, Liu H, Kojitani H, Wang S C. 2013. Vibrational mode analysis and heat capacity calculation of $K_2SiSi_3O_9$-wadeite. Phys Chem Miner, 40: 563–574

Cookenboo H, Bustin R, Wilks K. 1997. Detrital chromian spinel compositions used to reconstruct the tectonic setting of provenance: Implications for orogeny in the Canadian Cordillera. J Sediment Res, 67: 116–123

D'Arco P, Silvi B, Roetti C, Orlando R. 1991. Comparative study of spinel compounds: A pseudopotential periodic Hartree-Fock calculation of Mg_2SiO_4, Mg_2GeO_4, Al_2MgO_4, and Ga_2MgO_4. J Geophys Res, 96: 6107–6112

Deng L W, Liu X, Liu H, Zhang Y G. 2011. A first-principles study of the phase transition from Holl-I to Holl-II in the composition $KAlSi_3O_8$. Am Miner, 96: 974–982

Dick H J B, Bullen T. 1984. Chromian spinel as a petrogenetic indicator in abyssal and alpine-type peridotites and spatially associated lavas. Contrib Mineral Petrol, 86: 54–76

Duke J. 1983. Ore deposit models 7. Magmatic segregation deposits of chromite. Geosci Can, 10: 15–24

Fabries J. 1979. Spinel-olivine geothermometry in peridotites from ultramafic complexes. Contrib Mineral Petrol, 69: 329–336

Fei Y W, Ricolleau A, Frank M, Mibe K, Shen G Y, Prakapenka V. 2007. Toward an internally consistent pressure scale. Proc Natl Acad Sci USA, 104: 9182–9186

Gracia L, Beltrán A, Andrés J, Franco R, Recio J M. 2002. Quantum-mechanical simulation of $MgAl_2O_4$ under high pressure. Phys Rev B, 66: 224114

Graham J. 1978. Manganochromite, palladium antimonide, and some unusual mineral associations at the Nairne pyrite deposit, South Australia. Am Miner, 63: 1166–1174

Hazen R M, Finger L W. 1979. Bulk modulus-volume relationship for cation-anion polyhedra. J Geophys Res, 84: 6723–6728

Hill R J, Craig J R, Gibbs G V. 1979. Systematics of the spinel structure type. Phys Chem Miner, 4: 317–339

Hohenberg P, Kohn W. 1964. Inhomogeneous electron gas. Phys Rev, 136: 864–871

Howell D, Wood I G, Dobson D P, Jones A P, Nasdala L, Harris J W. 2010. Quantifying strain birefringence halos around inclusions in diamond. Contrib Mineral Petrol, 160: 705–717

Kagi H, Odake S, Fukura S, Zedgenizov D A. 2009. Raman spectroscopic estimation of depth of diamond origin: Technical developments and the application. Russ Geol Geophys, 50: 1183–1187

Karklit A, Stegantsev S, Petrova E. 1970. Properties of ceramics in the system $MgO-MgCr_2O_4$. Refract Ind Ceram, 11: 786–788

Klemme S, O'Neill H St C. 1997. The reaction $MgCr_2O_4 + SiO_2 = Cr_2O_3 + MgSiO_3$ and the free energy of formation of magnesiochromite ($MgCr_2O_4$). Contrib Mineral Petrol, 130: 59–65

Kohn W, Sham L J. 1965. Self-consistent equations including exchange and correlation effects. Phys Rev, 140: 1133–1138

Lee M H. 1995. Advanced pseudopotentials for large scale electronic structure calculations. Doctoral Dissertation. UK: University of Cambridge

Lenaz D, Logvinova A M, Princivalle F, Sobolev N V. 2009. Structural parameters of chromite included in diamond and kimberlites from Siberia: A new tool for discriminating source. Am Miner, 94: 1067–1070

Lenaz D, Skogby H, Princivalle F, Hålenius U. 2004. Structural changes and valence states in the $MgCr_2O_4$-$FeCr_2O_4$ solid solution series. Phys Chem Miner, 31: 633–642

Lin J S, Qteish A, Payne M C, Heine V. 1993. Optimized and transferable nonlocal separable ab initio pseudopotentials. Phys Rev B, 47: 4174–4180

Liu L G, Mernagh T P, Jaques A L. 1990. A mineralogical Raman spectroscopy study on eclogitic garnet inclusions in diamonds from Argyle. Contrib Mineral Petrol, 105: 156–161

Liu X, O'Neill H St C. 2004. The effect of Cr_2O_3 on the partial melting of spinel lherzolite in the system $CaO-MgO-Al_2O_3-SiO_2-Cr_2O_3$ at 1.1 GPa. J Petrol, 45: 2261–2286

Monkhorst H J, Pack J D. 1976. Special points for Brillouin-zone integrations. Phys Rev B, 13: 5188–5192

Nasdala L, Brenker F E, Glinnemann J, Hofmeister W, Gasparik T, Harris J W, Stachel T, Reese I. 2003. Spectroscopic 2D-tomography: Residual pressure and strain around mineral inclusions in diamonds. Eur J Mineral, 15: 931–935

Nestola F, Merli M, Nimis P, Parisatto M, Kopylova M, De Stefano A, Longo M, Ziberna L, Manghnani M. 2012. *In situ* analysis of garnet inclusion in diamond using single-crystal X-ray diffraction and X-ray micro-tomography. Eur J Mineral, 24: 599–606

Nestola F, Periotto B, Andreozzi G B, Bruschini E, Bosi F. 2014. Pressure-volume equation of state for chromite and magnesiochromite: A single-crystal X-ray diffraction investigation. Am Miner, 99: 1248–1253

O'Neill H St C. 1981. The transition between spinel lherzolite and garnet lherzolite, and its use as a geobarometer. Contrib Mineral Petrol, 77: 185–194

O'Neill H St C, Dollase W A. 1994. Crystal structures and cation distributions in simple spinels from powder XRD structural refinements: $MgCr_2O_4$, $ZnCr_2O_4$, Fe_3O_4 and the temperature dependence of the cation distribution in $ZnAl_2O_4$. Phys Chem Miner, 20: 541–555

O'Neill H St C, Navrotsky A. 1983. Simple spinels: Crystallographic parameters, cation radii, lattice energies, and cation distribution. Am Miner, 68: 181–194

O'Neill H St C, Wall V J. 1987. The olivine-orthopyroxene-spinel oxygen geobarometer, the nickel precipitation curve, and the oxygen fugacity of the Earth's upper mantle. J Petrol, 28: 1169–1191

Ottonello G, Civalleri B, Zuccolini M V, Zicovich-Wilson C M. 2007. Ab-initio thermal physics and Cr-isotopic fractionation of $MgCr_2O_4$. Am Miner, 92: 98–108

Paraskevopoulos G M, Economou M. 1981. Zoned Mn-rich chromite from podiform type chromite ore in serpentinites of northern Greece. Am Miner, 66: 1013–1019

Payne M C, Teter M P, Allen D C, Arias T A, Joannopoulos J D. 1992. Iterative minimization techniques for ab initio total-energy calculations: Molecular dynamics and conjugate gradients. Rev Mod Phys, 64: 1045–1097

Perdew J P, Burke K, Ernzerhof M. 1996. Generalized gradient approximation made simple. Phys Rev Lett, 77: 3865–3868

Perdew J P, Zunger A. 1981. Self-interaction correction to density-functional approximations for many-electron systems. Phys Rev B, 23: 5048–5079

Recio J M, Franco R, Pendás A M, Blanco M A, Pueyo L. 2001. Theoretical explanation of the uniform compressibility behavior observed in oxide spinels. Phys Rev B, 63: 184101

Rodríguez-Hernández P, Muñoz A. 2014. Theoretical ab initio calculations in spinels at high pressures. In: Manjon F J, Tiginyanu I, Ursaki V, eds. Pressure-Induced Phase Transitions in AB_2X_4 Chalcogenide Compounds. Springer Series in Materials Science, Vol 189. New York: Springer. 103–109

Smith F G. 1953. Historical development of inclusion thermometry. Toronto: University of Toronto Press

Stachel T, Harris J W. 2008. The origin of cratonic diamonds-constraints from mineral inclusions. Ore Geol Rev, 34: 5–32

Stephens P J, Devlin F J, Chabalowski C F, Frisch M J. 1994. Ab initio calculation of vibrational absorption and circular dichroism spectra using density functional force fields. J Phys Chem, 98: 11623–11627

Wang S C, Liu X, Fei Y W, He Q, Wang H J. 2012. *In situ* high-temperature powder X-ray diffraction study on the spinel solid solutions $(Mg_{1-x}Mn_x)Cr_2O_4$. Phys Chem Miner, 39: 189–198

Wang Z, O'Neill H St C, Lazor P, Saxena S K. 2002. High pressure Raman spectroscopic study of spinel $MgCr_2O_4$. J Phys Chem Solids, 63: 2057–2061

Xiong Z H, Liu X, Shieh S R, Wang S C, Chang L L, Tang J J, Hong X G, Zhang Z G, Wang H J. 2016. Some thermodynamic properties of larnite (β-Ca_2SiO_4) constrained by high *T*/*P* experiment and/or theoretical simulation. Am Miner, 101: 277–288

Yamanaka T, Takéuchi Y. 1983. Order-disorder transition in $MgAl_2O_4$ spinel at high temperatures up to 1700°C. Z Kristallogr, 165: 65–78

Yang J S, Dobrzhinetskaya L, Bai W J, Fang Q S, Robinson P T, Zhang J F, Green II H W. 2007. Diamond- and coesite-bearing chromitites from the Luobusa ophiolite, Tibet. Geology, 35: 875–878

Yong W J, Botis S, Shieh S R, Shi W G, Withers A C. 2012. Pressure-induced phase transition study of magnesiochromite ($MgCr_2O_4$) by Raman spectroscopy and X-ray diffraction. Phys Earth Planet Inter, 196-197: 75–82